Melting temperature of diamond and cubic boron nitride at 15 gigapascals

Akun Liang,[1] Yinjuan Liu,[1] Lanting Shi,[1,2] Li Lei,[1] Feng Zhang,[1] Qiwei Hu,[1] and Duanwei He[1,3,*]

[1]*Institute of Atomic and Molecular Physics, Sichuan University, Chengdu 610065, China*

[2]*Institute of Fluid Physics, Chinese Academy of Engineering Physics, Mianyang 621900, China*

[3]*Key Laboratory of High Energy Density Physics and Technology of Ministry of Education, Sichuan University, Chengdu 610065, China*

(Received 9 January 2019; revised manuscript received 26 September 2019; published 11 November 2019)

The melting temperature of diamond has not yet been experimentally measured under static pressure and these data for cubic boron nitride (cBN) are scarce. This lack of information is understandable due to the difficulty of heating optically transparent diamond via absorption of intense laser radiation in a diamond anvil cell and obtaining a high temperature with traditional resistance heating methods in a large-volume, multiple-anvil apparatus. Here, we report the melting temperature of diamond (5968 ± 457 K) and cBN (5689 ± 411 K) at a pressure of 15 GPa based on a two-stage multiple-anvil apparatus coupled with a so-called flash-heating method and show that the previous theoretical predictions underestimate the melting points of these two superhard materials. Our results indicate that diamond has the highest melting point in nature, and strengthen our understanding of the melting behavior of those two superhard materials.

DOI: 10.1103/PhysRevResearch.1.033090

I. INTRODUCTION

Diamond, the hardest known natural material and a well-known gemstone, is the main carbon form at high pressure and has attracted attention from physics, geology, materials science, and astrophysics researchers [1–5]. Diamond also has the highest reported thermal conductivity of all the natural materials because of its extremely strong covalent bonding between carbon atoms. Cubic boron nitride (cBN) has a crystal structure analogous to that of diamond, so these two materials have many similar properties, such as high hardness and melting points. Nonetheless, the melting points of diamond and cBN at static pressure are still a mystery because diamond and cBN are difficult to melt due to their high atomic density and strong covalent bonds. Although many papers have presented theoretical investigations on the melting line of diamond and cBN at ultrahigh pressure [6–10], experimental data are scarce as a consequence of the difficulty of reaching the extreme temperature required to melt diamond and cBN at high pressure in both a diamond anvil cell (DAC) and a large-volume, multiple-anvil apparatus with traditional heating methods.

Attempts have been made to determine the melting point of diamond and cBN at high pressure, but most of these attempts have only melted diamond without obtaining the exact melting temperature. Bundy [11] reported melting diamond, which was directly converted from well-crystallized graphite in a boron-doped graphite rod, employing a flash-heating method in a "belt" apparatus. Gold *et al.* [12] reported optical and scanning electron microscopy (SEM) images of a portion of a melted diamond anvil heated by a YAG laser. Togaya [13] investigated the melting behavior of diamond by heating boron-doped semiconducting diamond samples using flash heating with a bank of capacitors. Recently, Eggert *et al.* [14] revealed the melting curve of carbon at pressures in the range of 0.6–1.1 TPa generated by an OMEGA laser with 1-ns pulses and up to 3-kJ-driven shock compression. Moreover, the high sound velocities collected by Shaner *et al.* [15] associated with the insulating diamond phase determined by Mitchell *et al.* [16] indicated a positive dP/dT slope for the diamond-liquid phase line, which is opposite to the previous negative results by analogy with the melting curves of Si and Ge. Zerr and Boehler [17] measured the melting temperature of cBN at a pressure of 10 GPa, which combined the use of a CO_2-laser-heated DAC and *in situ* visual observation of large increases in temperature near the melting point of cBN, and the melting temperature is 3600 ± 100 K in their results.

II. EXPERIMENTS

A. Sample preparation

Diamond and cubic boron nitride (cBN) powders with a grain size of $6-8\,\mu$m and $5-6\,\mu$m, respectively (>99.9% purity, Zhongnan Jiete Superabrasives Co., Ltd., Zhengzhou, China) were used as the sample materials.

B. Flash-heating circuit and data collection

To reach the temperature required to melt diamond and cBN at 15 GPa, we used a high-purity spectroscopic graphite tube as a heater and heated the tube with a so called "flash-heating" method, which involved discharging a bank of capacitors (0.1 F) though the tube (Fig. 1). The heating energy was inserted in the graphite heater in less than 10 ms at a voltage

*Corresponding author: duanweihe@scu.edu.cn

Published by the American Physical Society under the terms of the Creative Commons Attribution 4.0 International license. Further distribution of this work must maintain attribution to the author(s) and the published article's title, journal citation, and DOI.

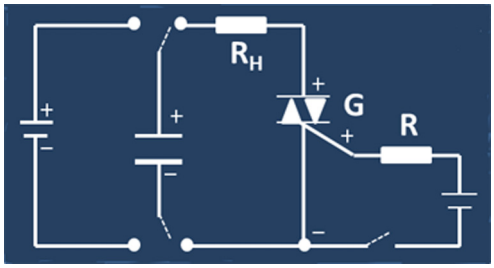

FIG. 1. Flash-heating circuit used in all of our experiments.

of 175 V and in less time when the voltage was lower. The flash-heating circuit includes three parts. First, the left part is a charge circuit, which is used to insert energy into the capacitor (0.1 F; in the middle) and reach the set voltage of the direct-current main (left; maximum voltage of 400 V). Then, the middle part is a discharging loop, which is used to transfer the energy from the capacitor to the graphite heater within 10 ms, and in this part, R_H represents the graphite heater, while G represents a thyristor. Finally, the right part is a control switch, which means the thyristor could be triggered by the current (0.2 A) produced by the right part to conduct and will continue to conduct until the current in the middle part decreases below the "holding current," approximately 13 A in our experiments.

A digital oscillograph, DL850E, produced by Yokogawa Electric Corporation was used to collected the voltage-time and current-time curves at various flash-heating voltages, and then, the resistance-time and inserted energy-time curves could be calculated by

$$R_t = \frac{U_t}{I_t} \quad \text{and} \quad E(t) = \int_0^t [I^2(t)R(t)]dt.$$

The frequency of the digital oscillograph is 10 MHz, which allowed the current and voltage data to be recorded with an interval of 0.1 μs, i.e., far faster than the flash-heating period (5–10 ms in our experiments).

C. High-pressure generation assembly

A two-stage multiple-anvil (Fig. 2) apparatus based on the DS6×8 MN cubic press developed at Sichuan University, including an anvil of tungsten carbide cubes with a truncation edge length of 4 mm, was used to generate the high pressure. The pressure was calibrated by the well-known pressure-induced phase transitions of Bi, Tl, Ba, ZnTe, and ZnS at room temperature, and a 10-mm MgO octahedron was used as the pressure medium. A high-purity spectroscopic graphite tube with an approximately 2.1-mm internal diameter and 3-mm outer diameter was used as the heater and surrounded by ZrO_2/18 mol% CaO. The samples were precompressed into rods with approximately 2.1-mm diameter and 6-mm length inside the graphite heater. Two graphite wafers, acting as electrodes, were loaded at each end of the graphite heater, and the pressure fluctuation during flash heating was within 0.4 GPa (Appendix C).

D. Raman test

A custom-built Raman system was used to collect Raman scattering spectra under normal conditions [18,19]. The

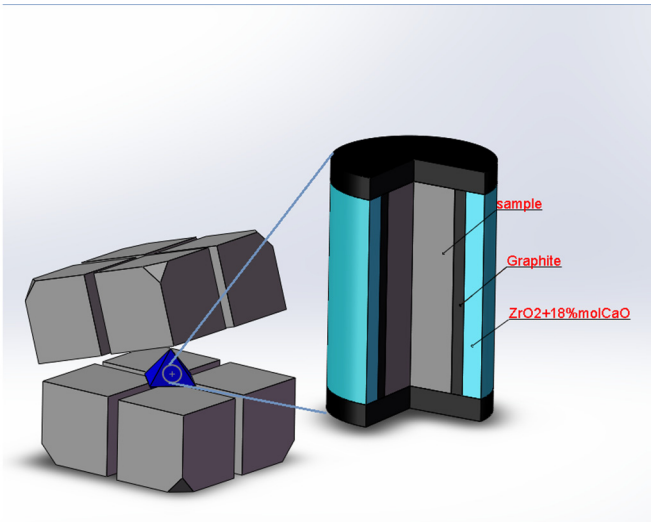

FIG. 2. The anvil of tungsten carbide cubes and sketch of the assembly.

system used a triple-grating monochromator (Andor Shamroch SR-303i-B, EU) with an attached EMCCD (Andor Newton DU970P-UVB, EU) and a solid-state laser (532 nm, RGB Laser System, Germany), and the Raman laser beam focused within ~5 μm on the sample surface.

III. RESULTS AND DISCUSSION

A. Melting diamond and cubic BN at high pressure

After flash heating at various voltages, the samples were examined with a scanning electron microscope (SEM). At relatively low voltages, such as 133 V [Fig. 3(a)], the diamond grains displayed a tendency to crack and fragment, and the grains displayed fracture rather than elastic deformation due to the deviatoric or shear stress in each individual grain derived from the high stress in the grain-to-grain contact areas under 15 GPa. Nevertheless, when the voltage was increased to a relatively high value, such as 220 V, the periphery of the diamond sample in direct contact with the graphite heater formed a significantly different microstructure. The diamond grains with an initial size of 6–8 μm underwent a grain-size reduction, which resulted in an average grain size of 100–200 nm. The grains were visually checked in the amplified image of the sample [Fig. 3(b)]. Nanocrystallization could be attributed to recrystallization from liquid diamond because the quenching rate in a flash-heating cycle is slower than that in a nucleation process [20] but comparable or even faster than that for grain growth. Thus, the onset of nanocrystallization was used as a criterion of diamond melting. This method was proven by Hrubiak *et al.* [21] by analyzing x-ray diffraction patterns of crystalline molybdenum quenched below and above its melting point. The continuous Debye diffraction rings were treated as evidence of newly crystallized fine grains in the sample when the temperature was above the melting point, while the presence of large diffraction spots signified a large-grained microstructure when the temperature was below the melting point. The flash-heating duration is essentially the same or even shorter than that for the

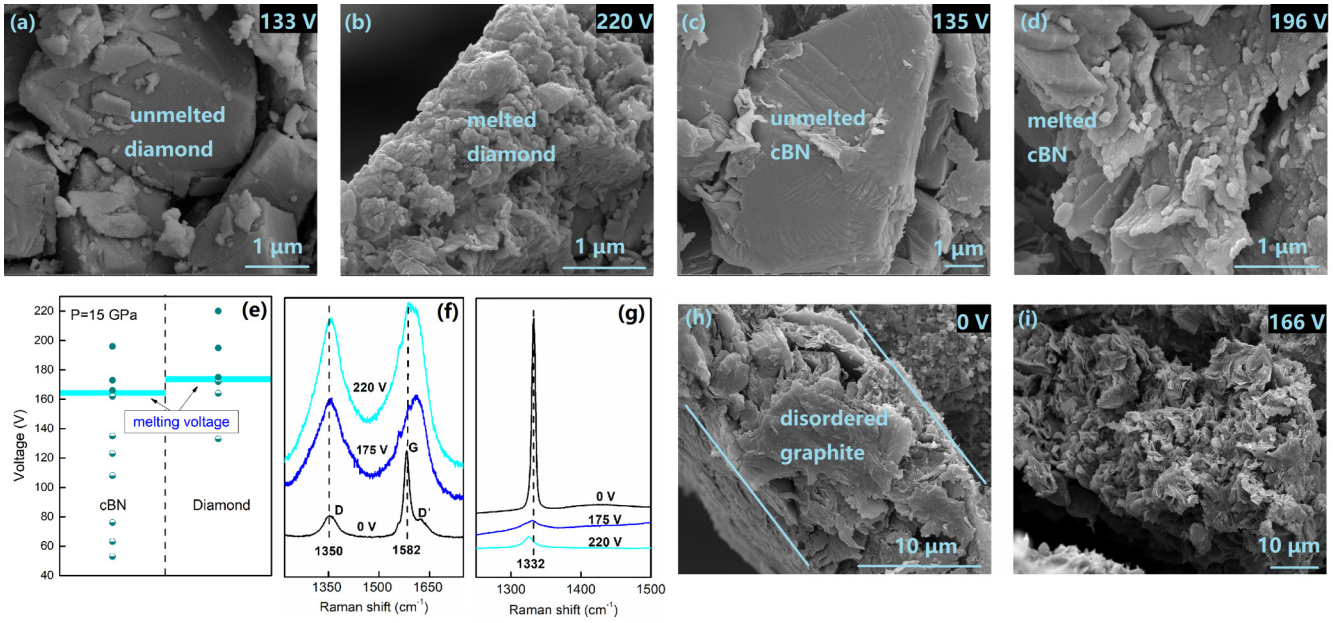

FIG. 3. SEM images of diamond and cBN after flash heating under 15 GPa. The flash-heating voltage is (a) 133 V and (b) 220 V for diamond and (c) 135 V and (d) 196 V for cBN; the nanocrystallization of diamond (b) and cBN (d) is used as evidence of melting. (e) A series of flash heating applied to diamond and cBN with a variety of voltages; the half-filled circles represent that a reduction in the grain size was not found in the sample, while the solid circles correspond to the appearance of nanocrystallization. Raman spectra for (f) graphite and (g) diamond; voltages of 175 V and 220 V were sufficient for diamond melting. SEM image (i) of the graphite heater with a flash-heating voltage of 166 V shows a smaller grain size and radial trace of the crystal structure compared with the SEM image of the heater with 0 V (h) and identified the melting history of graphite.

laser-heating DAC pulse (5–20 ms), and so the effects of chemical reactions between the molten sample and the graphite heater are probably minimal or nonexistent; we can see this from the full Raman spectra and XRD pattern of graphite recovered from 15 GPa and 220 V (Figs. 4 and 8). Figure 4 shows the full Raman spectra of graphite recovered from 15 GPa and 220 V and the initial graphite. The identification of the D, G, D', and G' bands is by comparing the Raman spectra of our work and Pimenta's work [22]. The peak with an asterisk (*) comes from the Raman mode of N_2 gas present in the air surrounding the sample; we can see that the Raman feature remains constant. The peak in the recovered sample becomes broader compared with the initial one; we attributed this change to the residual stress in the graphite heater resulting from high-pressure experiments.

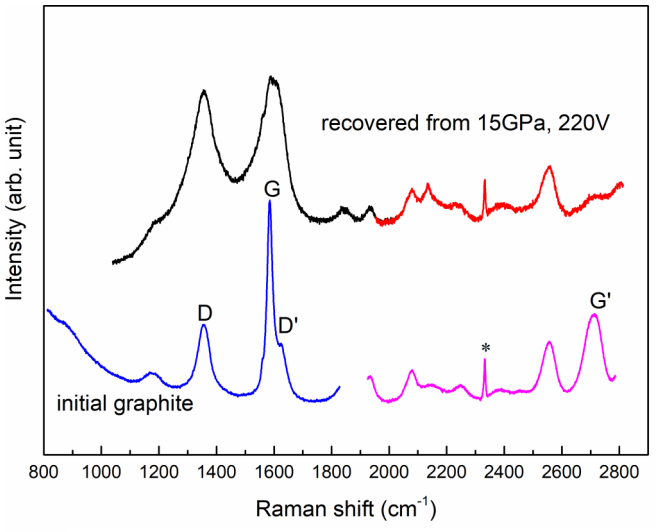

FIG. 4. Full Raman spectra of initial graphite heater and recovered from 15 GPa and 220 V.

Additionally, the grain sizes of cBN with flash-heating voltages of 135 V [Fig. 3(c)] and 196 V [Fig. 3(d)] were the same as those observed in diamond. In short, the changes that occurred in the microstructures of diamond and cBN revealed the melting behavior during a flash-heating period under 15 GPa. The results for a series of flash-heating voltages applied to these two materials are displayed in Fig. 3(e), which shows that the voltage required to melt diamond and cBN is 174 ± 1 V and 164 ± 2 V, respectively.

B. Evidence of no phase transition in graphite heater after flash heating

Raman scattering spectra [Fig. 3, panels (f) and (g)] of the diamond and graphite heater after flash heating with voltages of 175 V and 220 V were collected under normal conditions. Phase transition did not occur in either the diamond or graphite Raman spectra even though the temperature reached the melting point of diamond under 15 GPa. The reason for the absence of this phenomenon, i.e., the direct conversion of well-crystallized graphite into diamond discovered by Bundy [11], is assumed to be the difference in the graphite, which was molded by compressing the graphite powder used in our experiments. The residual stress in the graphite resulted in the G band shifting to a higher frequency and the D and G

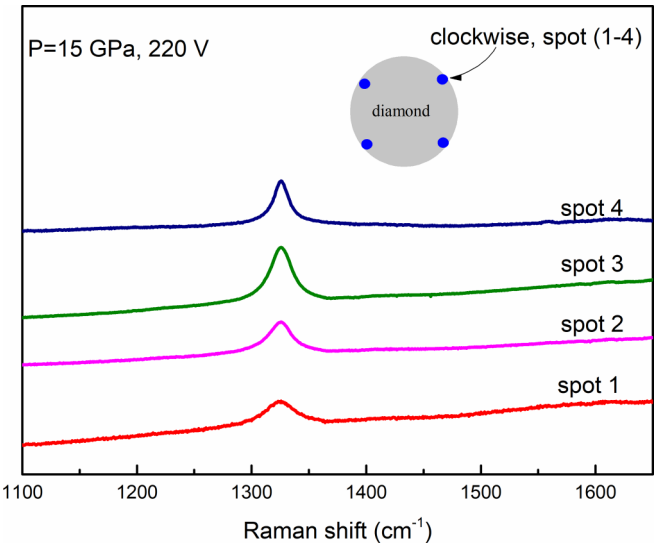

FIG. 5. Raman spectra of diamond quenched after flash-heating experiments at 220 V at four test spots.

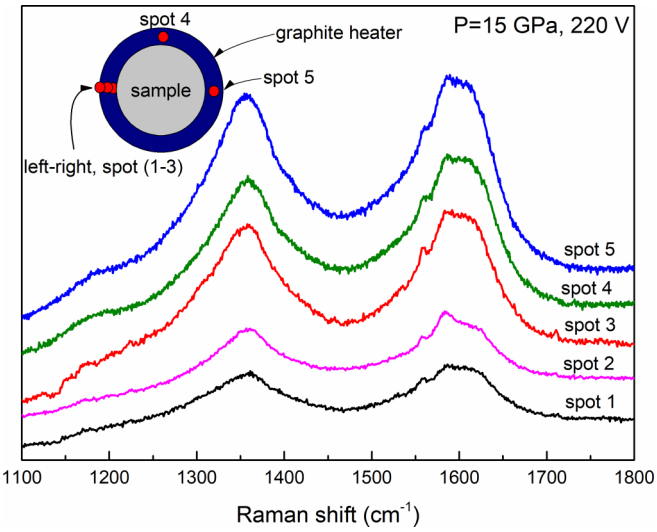

FIG. 6. Raman spectra of the graphite heater quenched after flash-heating experiments at 220 V at five test spots.

bands broadening, and the linewidth significantly increased with the increase in pressure and showed large hysteresis after the pressure was released [23]. Additionally, an apparent increase in the intensity ratio I_D/I_G of the D band and G band was observed, and an increase in the ratio is an indicator of a reduction in the graphite grain size and an increase in the number of crystallite edges the laser can reach [24]. These indications, such as the change in the grain size, agreed with the changes observed in the SEM images of the graphite subjected to flash heating with 0 V and 166 V in Fig. 3, panels (h) and (i). When the voltage was 166 V, a decrease in the direction and appearance of the radial trace of the crystal structure in the center was observed compared with that observed with 0 V. Bundy [25] observed the same radial trace in a melted graphite rod at high pressure. Thus, the graphite heater must go through a melting process before melting the diamond and cBN. The peak collected from diamond after 220-V flash heating shifting to lower frequency is attributed to size reduction of diamond [26], which is consistent with the SEM results.

All four or five test spots were conducted on graphite and diamond. The Raman spectra of the graphite and diamond, quenched from the flash-heating experiments with a voltage of 220 V (Figs. 5 and 6), from those test spots were unanimous in their agreement.

In the time-resistance curve in Fig. 7(c), we found that the curve at 127 V is the same with that in Bundy's flash-heating experiments [Fig. 7(b)] in which a flash-heating method combined with a spectroscopy graphite rod was used to explore the melting energy of graphite under high pressure, and the curve at 127 V is totally different from Bundy's other work, which indicated an irreversible graphite-to-diamond transition at about 12.5 GPa and 3000 K (produced by a flash-heating technique). This transition induced a rapid upward trend at the end of the time-resistance curve [Fig. 7(a)] and reached an open circuit. Actually, in all of our flash-heating experiments, we did not find the rapid upward trend at the end of the time-resistance curve (Fig. 9). On the contrary, the resistance of the graphite heater at the end of the flash heating is lower than the initial one at each flash-heating voltage. The absence of the graphite-to-diamond transition in our opinion is because of the difference of the graphite: a well-crystallized graphite in Bundy's experiment but molded by compressing the graphite powder in our experiment. The graphite-to-diamond phase transition happening at different pressure and temperature also could be found in the shock-induced graphite-to-diamond phase transition for pyrolytic, Ceylon natural, and synthetic graphite [27].

Figure 8 shows the XRD pattern of the graphite heater recovered from high-pressure and high-voltage heating experiments, while the inset shows the XRD pattern of the initial graphite heater; there is no sign of the occurrence of diamond or another phase, such as hexagonal graphite. Actually, there is a set of living examples which show nonequilibrium physical pathways because of the ultrafast heating time: (1) For graphite, slow heating of the solid can only sublime into the gas phase but not the liquid state at ambient pressures, but the liquid phase can be reached at ambient pressure by using short-pulse laser or flash heating with a discharge of a bank of capacitance [28–31], which allows for rapid heating of the solid phase. (2) The formation of diamond on the laser-driven shock experiment happened above 55 GPa due to a density jump [32] and 30 GPa on the explosive shock experiment [33], which is far beyond the graphite-diamond equilibrium boundary. (3) The pressure and temperature of the experiment on the ultrafast melting of carbon induced by intense proton beams could be up to 60 GPa and 20 000 K [34], which is in the liquid diamond region in the equilibrium carbon diagram. (4) By flash heating, graphite was melted in the diamond stable P-T field under 15 GPa [35].

C. Graphite resistance

The relationship between the resistance of graphite and time during a flash-heating cycle with a variety of voltages is illustrated in Fig. 9, and each curve includes the first 35 ms

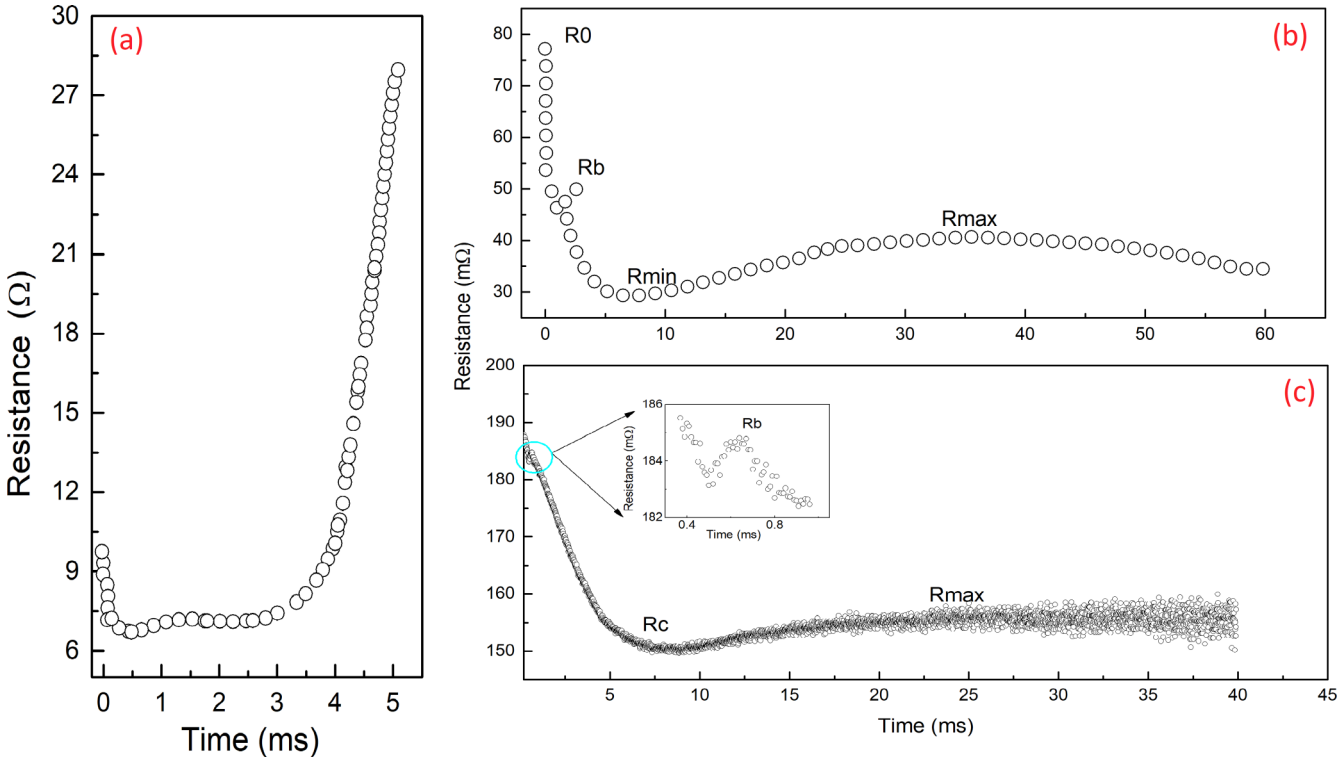

FIG. 7. (a) The time-resistance curve for spectroscopic graphite bar at 13 GPa in Bundy's work [11]. (b) The time-resistance curve for the initial 100-V flash heat on spectroscopic rod graphite at 4.8 GPa in Bundy's work [25]. (c) The time-resistance curve for the molded graphite by compressing the graphite powder in our work when the flash-heating voltage is 127 V and the pressure is 15 GPa.

of the flash-heating cycle. Compared with Bundy's work [25], the resistance curve evolved as the voltage increased, and several stages of the evolution of the resistance are evident from the curves. First, the resistance normally decreased at voltages of 56 V and 79 V as the traditional heat was conducted to the graphite heater at high pressure. Following that, the appearance of a slight increase after the first decrease indicated that between a voltage of 93 V and 106 V, graphite entered a stage between the end of the first decrease and the beginning of the break point, R_b, caused by the graphite melting. After that, the beginning sign of melting was observed at voltages of 108 V and 119 V as a second decrease in the resistance, and the signal for the maximum amount of graphite melting was observed at a voltage of 127 V. Finally, the resistance curves for voltages 131 V and 175 V represent the continuation of heating after the graphite is totally transformed into the liquid phase. Furthermore, when the voltage was 131 V and 175 V, the resistance of graphite decreased slowly from approximately 4 or 10 ms, and this decrease could be attributed to the quenching of liquid graphite but not the phase transition from a solid to liquid, such as the transition in the curve at 127 V. The rate at which the energy is conducted into the graphite heater will increase followed by an increase in the voltage before reaching a plateau, which could be observed in the energy versus time curve (Fig. 10). The value of R_b, consequently, in the resistance curves of 131 V and 175 V was earlier than that in the 127 V curve. To sum up, the graphite heater melted from 107 ± 1 V to 129 ± 2 V, which is below the voltages needed to melt diamond and cBN.

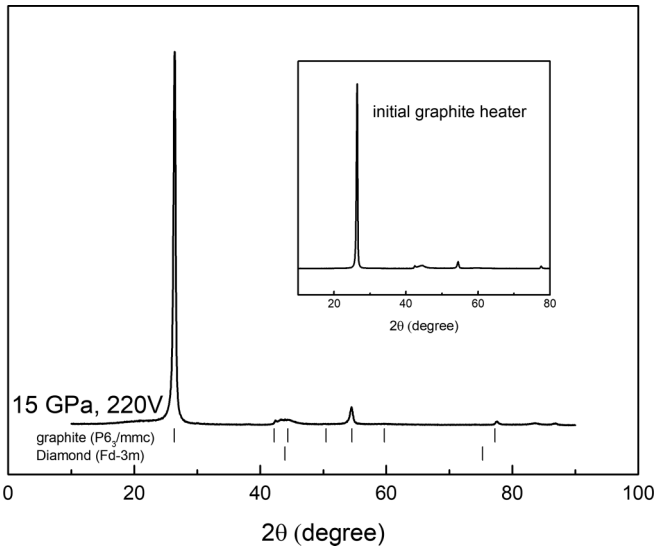

FIG. 8. XRD pattern of graphite heater recovered from 15 GPa and 220 V of flash heating and the initial graphite heater.

D. Melting-temperature determination

Materials, including NaCl, KCl, Al_2O_3, and MgO with melting temperatures at a pressure of 15 GPa of 1992 ± 62 K [36], 2800 ± 40 K [37], 3290 ± 120 K [38], and 4150 ± 255 K [39], respectively, were selected for a temperature calibration to establish the relationship between the

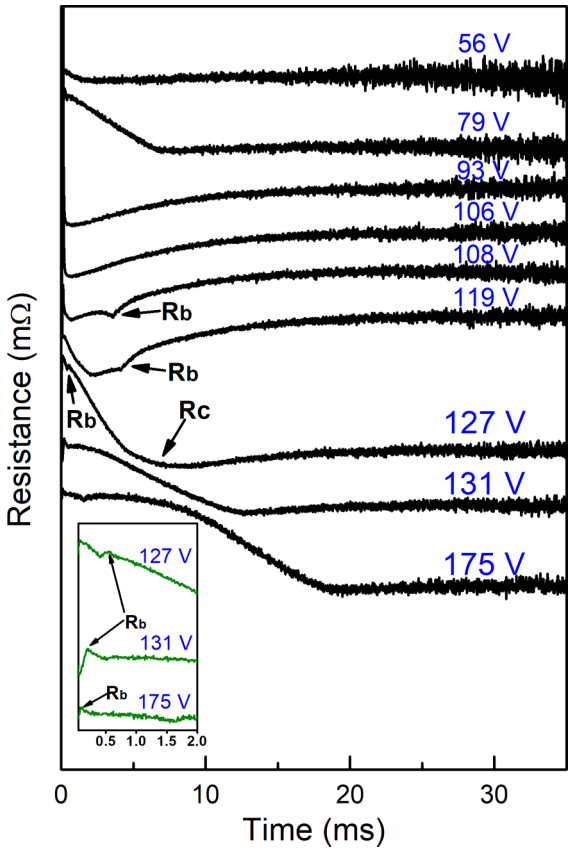

FIG. 9. Curves of time versus resistance of graphite with different voltages at a pressure of 15 GPa.

flash-heating voltage and the temperature in the periphery of the sample (T_P). The melting temperature of KCl was deduced from the data reported by Boehler with the Simon equation [40] (Fig. 11) (Appendix B), because the minimum pressure

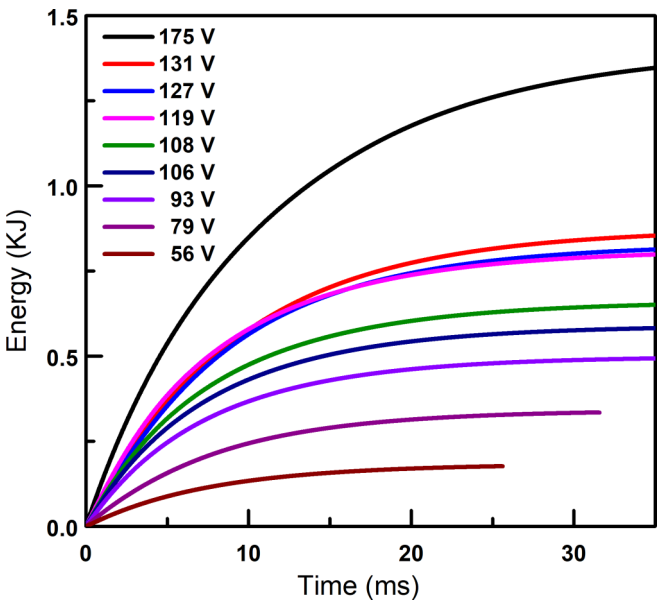

FIG. 10. Curves of time versus inserted energy of graphite with different voltages at a pressure of 15 GPa.

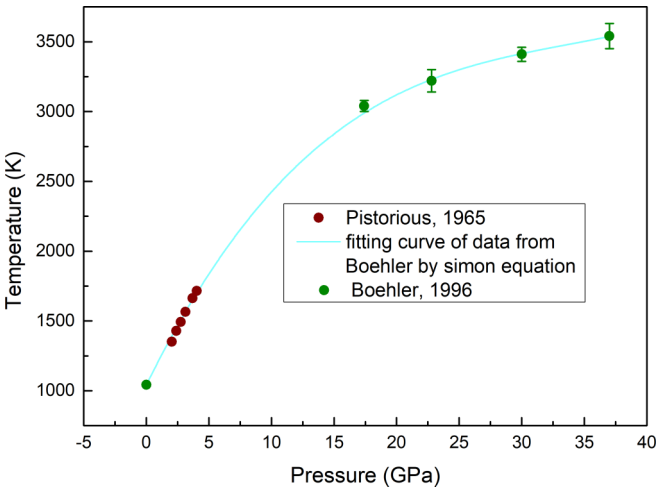

FIG. 11. Melting temperature of KCl reported by Boehler in 1996 [37] (green solid circle) and Pistorius in 1965 [65] (brown solid circle).

data in that work is 17.8 GPa. The melting temperature of MgO, worth mentioning particularly, is an elusive and controversial topic because of the significant discrepancies between the published experimental data [39,41–43] and computational data [44–47]. A set of recent experimental studies [39,41,43] showed a higher melting temperature than the first experimental value reported by Zerr *et al.* [42] (Fig. 12), and recent shock compression experiments [48] show consistency with the high melting slope of experimental and theoretical results but not the results of Zerr and Boehler's experiments. We chose the value reported by Kimura *et al.* [39] who pointed out that the misjudgment existed in earlier work that underestimated the melting temperature of MgO based on an analysis of the microtexture of quenched samples, which is similar to the means used to judge melting in samples in our experiments, but the error range used in our fitting is ±255 K, not the ±200 K of Kimura's work, because we considered the

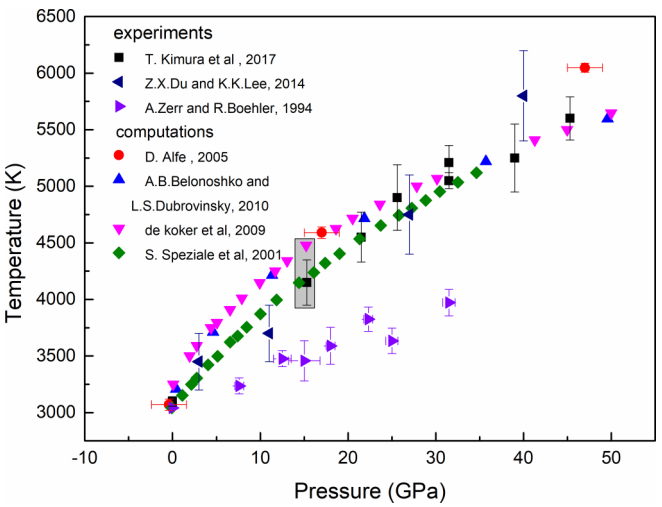

FIG. 12. Melting-temperature data obtained from results of different experiments and computations.

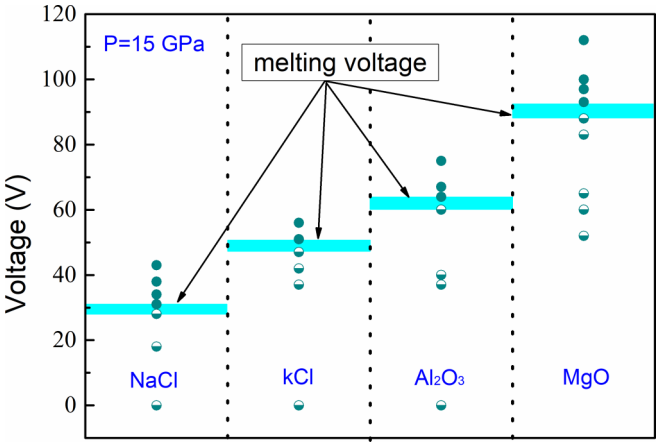

FIG. 13. A series of flash heating was conducted with NaCl, KCl, Al_2O_3, and MgO samples at a pressure of 15 GPa. Shots with melted sample are shown as solid circles, and half-filled circles represent unmelted samples after flash heating. This study determined that the voltage required to melt NaCl, KCl, Al_2O_3, and MgO was 29 ± 2 V, 49 ± 2 V, 62 ± 2 V, and 90.5 ± 2.5 V, respectively.

discrepancy of melting temperature at 15 GPa between the theoretical data and Kimura's data.

A series of flash-heating experiments were conducted, and the results are shown in Fig. 13. The method used to judge melting in a selected material after each shot with a given voltage was previously described, i.e., the first appearance of a grain size reduction or nanocrystallization in the SEM images.

Based on the obtained data on the required melting voltage for four materials (NaCl, KCl, Al_2O_3, and MgO) and their melting points at a pressure of 15 GPa, five points, including the starting point at 0 V and 300 K, were used to fit the linear relationship between $V^{3/4}$ and T_P (Fig. 14), and we treated T_P as a free parameter to fit our voltage data. As convective heat

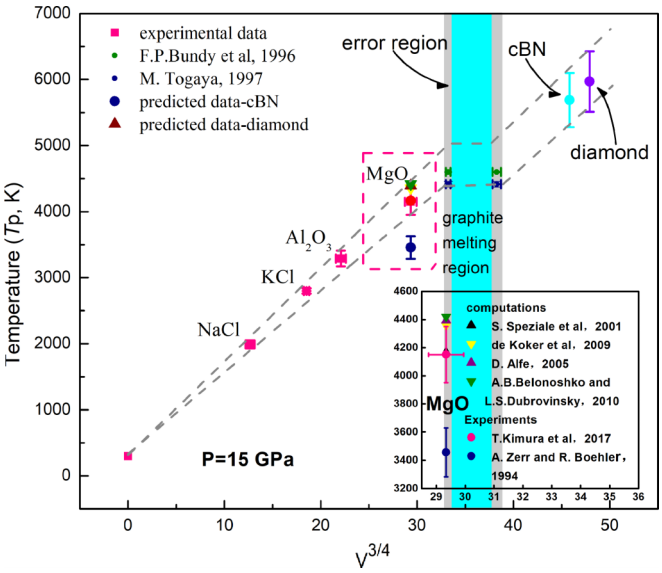

FIG. 14. The relationship between $V^{3/4}$ and temperature at the periphery of the sample (T_P) and the predicted melting temperature of diamond and cBN under 15 GPa.

transfer is the dominant form of heat transfer in liquid and gas, so heat conduction and thermal radiation are considered to be the main forms of heat transfer through the boundary between the graphite heater and the samples. This relationship can be used to quantitatively assess T_P when the voltage is below the melting voltage of MgO and to appropriately estimate the temperature associated with a given voltage below the voltage (107 ± 1 V) that initiates graphite melting. The graphite melting region was determined by an analysis of the time-resistance curve. More importantly, the resistance of the graphite heater remained relatively constant before and after melting according to the resistance-time curve at 175 V, which is presented in Fig. 9. Consequently, we introduced the same relationship observed below the graphite melting region when the voltage was above the graphite melting region. The melting point illustrated in the graphite melting region was obtained by extrapolating the melting curves measured by Bundy (green points) [49] and Togaya (blue points) [50] up to 15 GPa. Similarly, the melting lines determined by those researchers were also obtained by flash-heating a spectroscopic graphite rod at high pressure, and the unanimous agreement of the melting temperature of graphite and T_P in the graphite melting region in our fitting curve could be a sign that the linear fit between T_P and $V^{3/4}$ is reasonable.

IV. CONCLUSION

The results show that previous estimates of the melting points of diamond and cBN from theoretical calculations [6–8,10] are too low at a pressure of 15 GPa (Fig. 15). Likewise, the disagreement between the experimental data and the values calculated with density functional theory or the effective medium approximation for the melting temperature at high pressure was also observed in other studies [43,51]. Zerr's work [17] for the melting temperature of cBN under 10 GPa is also shown in Fig. 15. Some factors, including premelting of the sample and laser heating under extreme conditions, could affect the accuracy of the melting-point value, resulting in an underestimate of the melting temperature like what happened in MgO [43].

The melting points of not only diamond and cBN but also most high-melting-point materials (crystalline and insulative) within the pressure range of a multiple-anvil apparatus can be measured by the approach described in our paper. The melting points of diamond and cBN were experimentally obtained at 15 GPa, and this information could be used as a reference point for evaluating thermodynamics and calculating the melting points at high pressure. Furthermore, the results also have implications for the development of the carbon and boron nitride phase diagrams. Further work is still needed as the error range of the data in our work is large, and the data only cover one pressure point.

ACKNOWLEDGMENTS

This study was supported by the National Key R&D Program of China (No. 2018YFA0305900) and the National Natural Science Foundation of China (Grants No. 51472171 and No. 11427810).

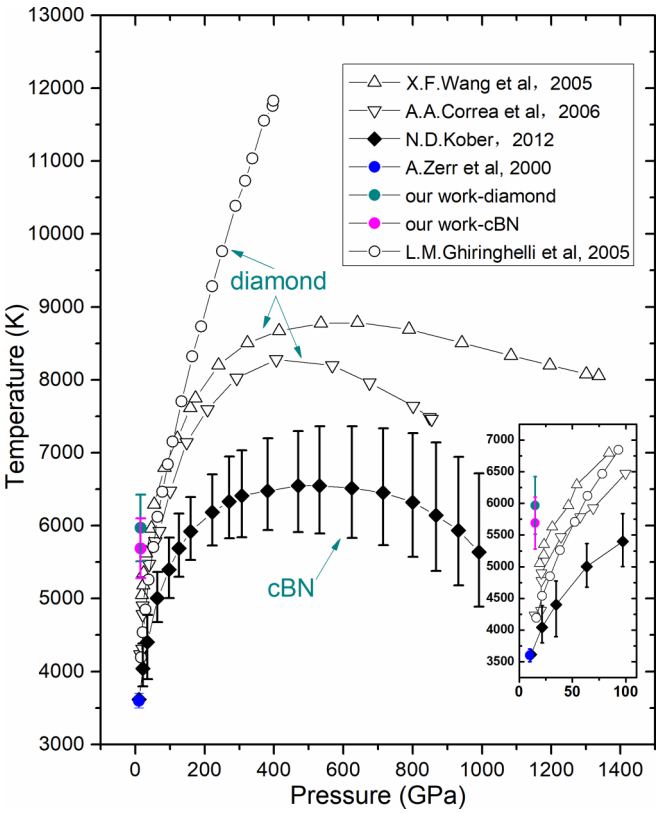

FIG. 15. The melting temperatures of diamond and cBN at a pressure of 15 GPa were determined to be 5968 ± 457 K and 5689 ± 411 K, respectively, in our experiments, and these values are approximately 1000 K higher than the theoretical simulation value published by Wang [8] and Correa [6] for diamond and approximately 1400 K higher than the value calculated by de Koker [10] for cBN.

APPENDIX A: MELTING HISTORY OF THE SAMPLES

After each flash-heating experiment, we chose the sample located exactly in the middle of the graphite tube for SEM examination. After each sample was quenched from the flash-heating cycle, SEM was utilized to carefully examine the periphery of the sample, and these microstructure images were used to judge sample melting by the means described in the article. In addition, the development of the sample morphology with the increase in the voltage can be observed in Fig. 16.

APPENDIX B: DETERMINATION OF THE MELTING TEMPERATURE OF KCl at 15 GPa

As shown in Fig. 11, because the minimum pressure of the measured data is 17.8 GPa in Boehler's work [37], we fitted the melting-temperature data of KCl reported by Boehler with the Simon equation [40]:

$$T_m = T_0\left(\frac{P_m}{A}+1\right)^{1/B},$$

where T_0 is the melting temperature at zero pressure, P_m is the corresponding pressure, and A and B are constants. We obtained $A = 0.0895$ and $B = 4.923$. We found the fitting curve in excellent agreement with the data measured by Pistorius in a piston-cylinder apparatus to 41 kbar, and agreement is also found with Boehler's paper. Then we obtained the melting temperature of KCl at 15 GPa from the fitting curve and the error was induced from the error existing in Boehler's data.

APPENDIX C: CALCULATION OF THE PRESSURE FLUCTUATION DURING FLASH HEATING

As the graphite is heated by the flash-heating method rapidly, it transforms to a liquid state and leads to a volume expansion. The assembly of the experiment can be found in Fig. 2. The volume fractions of $ZrO_2 + CaO$, the sample, graphite, and MgO are 9.5%, 4.4%, 5%, and 81.1%, respectively. The bulk moduli of these materials are 189 ± 15 GPa (unpublished data), 443 GPa (when the sample is diamond) [52], 36.5 GPa [53], and 177 ± 4 GPa [54], respectively, and then we arrive at an average bulk modulus of the whole assembly of about 182.8 GPa. The volume change of graphite from the solid state to the liquid state is unknown. But we know the thermal expansion of graphite during melting at low pressure (about 5.4 GPa) was less than 24% [55], and the greater the pressure, the graphite expands less during melting [56]. We chose the density of liquid graphite at 15 GPa from simulation results with quantum molecular dynamics [57]; the value is 2.4 g/cm^3. The density of solid graphite under 15 GPa was calculated from the initial density combining the Birch-Murnaghan equation [58,59]. Finally, a 6% volume change of graphite from the solid to liquid state at 15 GPa was calculated. According to the average bulk modulus and the volume change of graphite when it melts at high pressure, we adopt the Birch-Murnaghan equation to estimate the pressure change when graphite melting is at 15 GPa, and then we arrive at a pressure change of about 0.4 GPa when graphite melting is under 15 GPa. As the thermal expansion of graphite [60] is less than the volume change during melting, the pressure change before and after flash heating is less than 0.4 GPa.

APPENDIX D: HEAT TRANSFER IN DIFFERENT SAMPLES (DIAMOND, cBN, and MgO)

The classical Fourier heat transfer equation can be written as

$$\frac{\partial T}{\partial t} = a\left(\frac{\partial^2 T}{\partial x^2}+\frac{\partial^2 T}{\partial y^2}+\frac{\partial^2 T}{\partial z^2}\right)+\frac{q_v}{\rho c} \quad \text{or}$$

$$\frac{\partial T}{\partial t} = a\left(\frac{\partial^2 T}{\partial r^2}+\frac{1}{r}\frac{\partial T}{\partial r}+\frac{1}{r^2}\frac{\partial^2 T}{\partial \phi^2}+\frac{\partial^2 T}{\partial z^2}\right)+\frac{q_v}{\rho c},$$

where T is the temperature, $a = k/\rho c$ is the thermal diffusivity, ρ is the mass density, and c is the heat capacity of the material.

Because of the symmetry of the cylindrical assembly (Fig. 17) and that we neglect the heat conduction in the axial direction, the temperature T is defined here as a function of $T(r, t)$. Then $T(r, t)$ can be expressed as

$$\frac{\partial T}{\partial t} = a\left(\frac{\partial^2 T}{\partial r^2}+\frac{1}{r}\frac{\partial T}{\partial r}\right)+\frac{q_v}{\rho c}.$$

Here, the increasing of the graphite temperature is a time- and power-dependent quantity. The solution of this issue is

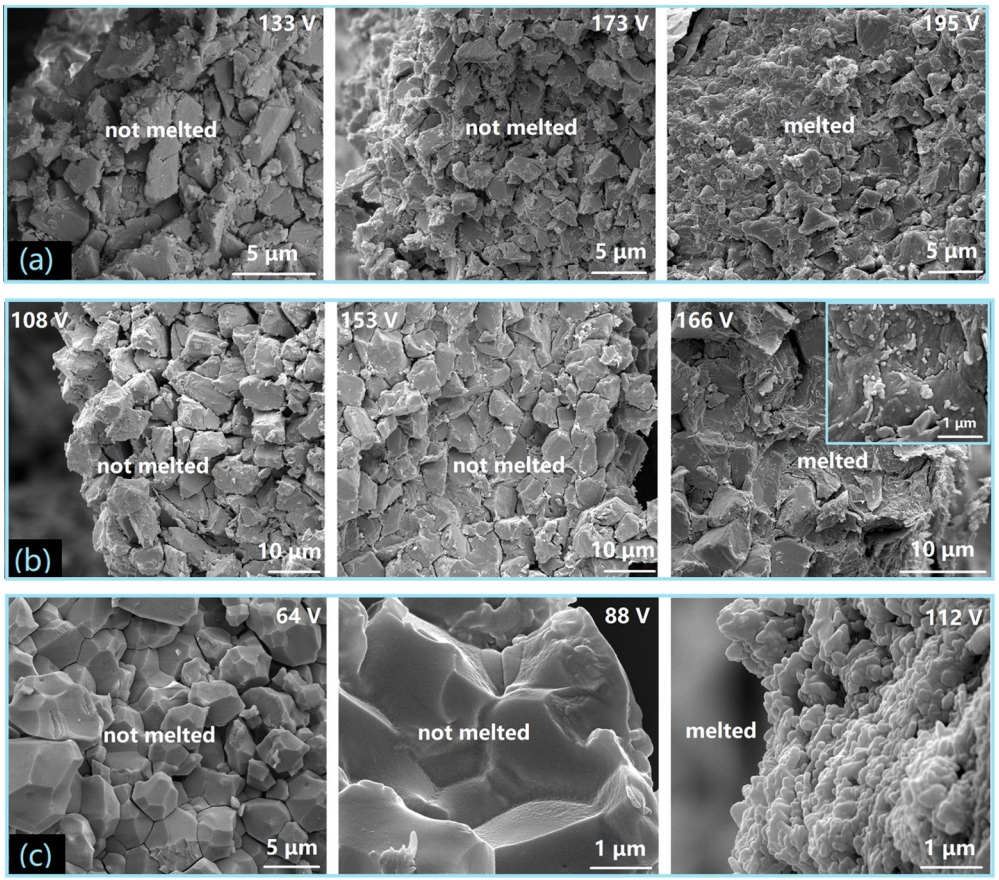

FIG. 16. Micromorphology of diamond (a), cBN (b), and MgO (c) after flash heating at various voltages under a pressure of 15 GPa. The changes can reveal the melt history of them.

remarkably difficult, so we treat the graphite temperature as a constant average value and the duration is 3 ms. The time of the increase of the temperature can be read from the time-resistance curve; actually, the increasing-temperature time is less than 3 ms when the voltage is higher, but we neglect the time change and treat it as the same.

So the Fourier heat transfer equation we adopt in our calculation is

$$\frac{\partial T}{\partial t} = a\left(\frac{\partial^2 T}{\partial r^2} + \frac{1}{r}\frac{\partial T}{\partial r}\right). \tag{D1}$$

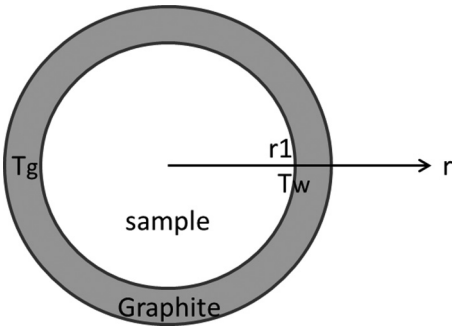

FIG. 17. Schematic diagram of the calculation of heat transfer in different samples.

The initial condition yields

$$T\ (r,t)|_{t=0} = T_0.$$

The boundary conditions are adiabatic as

$$\left.\frac{\partial T(r,t)}{\partial r}\right|_{r=0} = 0 \quad \text{and} \quad -k\left.\frac{\partial T\ (r,t)}{\partial r}\right|_{r=r_1} = \alpha(T_w - T_g)|_{r=r_1},$$

where α is the rate of the heat exchange between the sample and graphite heater, T_w is the temperature at the boundary between the sample and graphite heater, and T_g is the temperature of the graphite.

Then, the solution of Eq. (D1) with initial and boundary conditions can be written as

$$\varphi = 2\sum_{n=1}^{\infty} \theta^{-\mu_n^2 F_0} \frac{\sin\mu_n \cos\mu_n R}{\mu_n + \sin\mu_n \cos\mu_n},$$

where $\varphi = \frac{\theta}{\theta_1} = \frac{T-T_g}{T_0-T_g}$, $F_0 = \frac{at}{r_1^2}$, $R = \frac{r}{r_1}$, $B_i = \frac{\alpha r_1}{k}$, and B_i meet the characteristic equation

$$\frac{\mu}{B_i} = ctg\mu.$$

μ_n $(n = 1, 2, 3, \ldots)$ is the nth root of this equation. As the sample is impinging on the graphite heater and the distance between them is tiny, we can assume that the rate of the heat exchange between them is infinite, so B_i is tending to zero.

TABLE I. Thermal parameter of diamond and MgO used in our heat transfer calculations.

Material	Parameter	Value	Reference
Diamond	Heat capacity c (J/K kg)	2000	[61]
	Coefficient of heat conductivity k (W/m K)	551	[62]
	Density ρ (kg/m^3)	3500	
MgO	Heat capacity c (J/K kg)	1250	[63]
	Coefficient of heat conductivity k (W/m K)	15	[64]
	Density ρ (kg/m^3)	3580	

Then we can obtain the ratio between Q_i and Q, where Q represents the heat transfer to the sample from $t = 0$ to $t = i$ while Q is the total heat from $t = 0$ to $t = \infty$.

Thermal parameters used in our calculation can be found in Table I; our result is that the ratio of Q_i to Q is 12.3% when the sample is diamond and 6% when the sample is MgO. The temperature in the sample center remains unchanged in both of these conditions.

So it seems that the total transferred heat in diamond is 6% higher during the temperature-increasing process. If we also adopt 6% heat loss in the diamond sample, then the melting voltage of diamond should be 168 V, which is only 6 V lower than the 174 V determined in our experiment. Since there are some assumption (we adopt no temperature-dependent heat capacity and coefficient of heat conductivity, we do not consider the effect of the grain boundary in the coefficient of heat conductivity, and so on), we do not add this correction in our melting voltage for diamond, but demonstrate that the difference is negligible. Since the coefficient of heat conductivity of cBN is lower than diamond, the difference between cBN and MgO is lower than 6%.

[1] F. P. Bundy, Physica A **156**, 169 (1989).
[2] J. S. Dickey, W. A. Bassett, J. M. Bird, and M. S. Weathers, Geology **11**, 219 (1983).
[3] H.-K. Mao, X.-J. Chen, Y. Ding, B. Li, and L. Wang, Rev. Mod. Phys. **90**, 015007 (2018).
[4] T. Irifune, A. Kurio, S. Sakamoto, T. Inoue, and H. Sumiya, Nature (London) **421**, 599 (2003).
[5] M. Ross, Nature (London) **292**, 435 (1981).
[6] A. A. Correa, S. A. Bonev, and G. Galli, Proc. Natl. Acad. Sci. USA **103**, 1204 (2006).
[7] L. M. Ghiringhelli, J. H. Los, E. J. Meijer, A. Fasolino, and D. Frenkel, Phys. Rev. Lett. **94**, 145701 (2005).
[8] X. F. Wang, S. Scandolo, and R. Car, Phys. Rev. Lett. **95**, 185701 (2005).
[9] M. Hanfland, K. Syassen, and R. Sonnenschein, Phys. Rev. B **40**, 1951 (1989).
[10] N. de Koker, J. Phys.: Condens. Matter **24**, 055401 (2012).
[11] F. P. Bundy, J. Chem. Phys. **38**, 631 (1963).
[12] J. S. Gold, W. A. Bassett, M. S. Weathers, and J. M. Bird, Science **225**, 921 (1984).
[13] M. Togaya, in *Science and Technology of New Diamond*, edited by O. F. S. Saito and M. Yoshikawa (KTK Scientific Publishers, Tokyo, 1990), p. 369.
[14] J. H. Eggert, D. G. Hicks, P. M. Celliers, D. K. Bradley, R. S. McWilliams, R. Jeanloz, J. E. Miller, T. R. Boehly, and G. W. Collins, Nat. Phys. **6**, 40 (2010).
[15] J. W. Shaner, J. M. Brown, C. A. Swenson, and R. G. Mcqueen, J. Phys. (Paris) **45**, 235 (1984).
[16] A. C. Mitchell, J. W. Shaner, and R. N. Keeler, Physica B+C **139**, 386 (1986).
[17] A. Zerr, G. Serghiou, and R. Boehler, in *Handbook of Ceramic Hard Materials* (Wiley-VCH, Weinheim, 2000), pp. 41–64.
[18] Y. J. Liu, D. W. He, Z. L. Kou, F. M. Liu, P. Wang, Q. W. Hu, and A. K. Liang, Scr. Mater. **149**, 1 (2018).
[19] L. J. Tan, Q. W. Hu, L. Lei, X. D. Jiang, S. P. Gao, and D. W. He, J. Appl. Phys. **118**, 185903 (2015).
[20] Y. Shibuta, K. Oguchi, T. Takaki, and M. Ohno, Sci. Rep. **5**, 13534 (2015).
[21] R. Hrubiak, Y. Meng, and G. Y. Shen, Nat. Commun. **8**, 14562 (2017).
[22] M. A. Pimenta, G. Dresselhaus, M. S. Dresselhaus, L. G. Cancado, A. Jorio, and R. Saito, Phys. Chem. Chem. Phys. **9**, 1276 (2007).
[23] M. Hanfland, H. Beister, and K. Syassen, Phys. Rev. B **39**, 12598 (1989).
[24] D. S. Knight and W. B. White, J. Mater. Res. **4**, 385 (1989).
[25] F. P. Bundy, J. Chem. Phys. **38**, 618 (1963).
[26] A. C. Ferrari and J. Robertson, Philos. Trans. R. Soc. A **362**, 2477 (2004).
[27] W. H. Gust, Phys. Rev. B **22**, 4744 (1980).
[28] J. Steinbeck, G. Braunstein, M. S. Dresselhaus, T. Venkatesan, and D. C. Jacobson, J. Appl. Phys. **58**, 4374 (1985).
[29] A. M. Malvezzi, N. Bloembergen, and C. Y. Huang, Phys. Rev. Lett. **57**, 146 (1986).
[30] O. P. Watts and C. E. Mendenhall, Phys. Rev. (Series I) **33**, 65 (1911).
[31] O. P. Watts and C. E. Mendenhall, Ann. Phys. (Berlin) **340**, 783 (1911).
[32] D. Kraus *et al.*, Nat. Commun. **7**, 10970 (2016).
[33] P. S. Decarli and J. C. Jamieson, Science **133**, 1821 (1961).
[34] A. Pelka *et al.*, Phys. Rev. Lett. **105**, 265701 (2010).
[35] M. Togaya, High-Pressure Sci. Technol. **4**, 342 (1990).
[36] R. Boehler, M. Ross, and D. B. Boercker, Phys. Rev. Lett. **78**, 4589 (1997).
[37] R. Boehler, M. Ross, and D. B. Boercker, Phys. Rev. B **53**, 556 (1996).
[38] G. Y. Shen and P. Lazor, J. Geophys. Res.: Solid Earth **100**, 17699 (1995).
[39] T. Kimura, H. Ohfuji, M. Nishi, and T. Irifune, Nat. Commun. **8**, 15735 (2017).
[40] F. Simon and G. Glatzel, Z. Anorg. Allg. Chem. **178**, 309 (1929).
[41] Z. X. Du and K. K. M. Lee, Geophys. Res. Lett. **41**, 8061 (2014).
[42] A. Zerr and R. Boehler, Nature (London) **371**, 506 (1994).
[43] L. Zhang and Y. W. Fei, Geophys. Res. Lett. **35**, L13302 (2008).

[44] D. Alfe, Phys. Rev. Lett. **94**, 235701 (2005).
[45] A. B. Belonoshko and L. S. Dubrovinsky, Geochim. Cosmochim. Acta **60**, 1645 (1996).
[46] N. de Koker and L. Stixrude, Geophys. J. Int. **178**, 162 (2009).
[47] S. Speziale, C. S. Zha, T. S. Duffy, R. J. Hemley, and H. K. Mao, J. Geophys. Res.: Solid Earth **106**, 515 (2001).
[48] R. S. McWilliams, D. K. Spaulding, J. H. Eggert, P. M. Celliers, D. G. Hicks, R. F. Smith, G. W. Collins, and R. Jeanloz, Science **338**, 1330 (2012).
[49] F. P. Bundy, W. A. Bassett, M. S. Weathers, R. J. Hemley, H. K. Mao, and A. F. Goncharov, Carbon **34**, 141 (1996).
[50] M. Togaya, Phys. Rev. Lett. **79**, 2474 (1997).
[51] A. Dewaele, M. Mezouar, N. Guignot, and P. Loubeyre, Phys. Rev. Lett. **104**, 255701 (2010).
[52] I. V. Aleksandrov, A. F. Goncharov, A. N. Zisman, and S. M. Stishov, Zh. Eksp. Teor. Fiz. **93**, 680 (1987).
[53] Y. X. Zhao and I. L. Spain, Phys. Rev. B **40**, 993 (1989).
[54] T. S. Duffy, R. J. Hemley, and H. K. Mao, Phys. Rev. Lett. **74**, 1371 (1995).
[55] S. V. Lebedev and A. I. Savvatimskiy, in *Investigation of Metals and Graphite under Conditions of Rapid Electric Heating* (Harwood Academic, New York, 1993), pp. 1–79.
[56] A. I. Savvatimskiy, J. Phys.: Condens. Matter **20**, 114112 (2008).
[57] V. S. Dozhdikov, A. Y. Basharin, P. R. Levashov, and D. V. Minakov, J. Chem. Phys. **147**, 214302 (2017).
[58] F. D. Murnaghan, Proc. Natl. Acad. Sci. USA **30**, 244 (1944).
[59] F. Birch, Phys. Rev. **71**, 809 (1947).
[60] R. Berman and F. Simon, Z. Elektrochem. **59**, 333 (1955).
[61] N. Mounet and N. Marzari, Phys. Rev. B **71**, 205214 (2005).
[62] W. L. Liu, M. Shamsa, I. Calizo, A. A. Balandin, V. Ralchenko, A. Popovich, and A. Saveliev, Appl. Phys. Lett. **89**, 171915 (2006).
[63] M. H. G. Jacobs and H. A. J. Oonk, Phys. Chem. Chem. Phys. **2**, 2641 (2000).
[64] S. Stackhouse, L. Stixrude, and B. B. Karki, Phys. Rev. Lett. **104**, 208501 (2010).
[65] C. W. F. T. Pistorius, J. Phys. Chem. Solids **26**, 1543 (1965).